Multilayer analytical model for vertical ground heat exchanger with groundwater flow

Selçuk Erol[a,b,c], Bertrand François[a,*]

[a] Université Libre de Bruxelles (ULB) Building, Architecture and Town Planning Dept (BATir), Laboratoire de GéoMécanique, Avenue F.D. Roosevelt, 50 – CPI 194/2, B – 1050 Bruxelles, Belgium
[b] Flemish Institute of Technological Research (VITO), Boeretang 200, 2400 Mol, Belgium
[c] Department of Earth and Environmental Sciences, Celestijnenlaan 200E, KU Leuven, 3001 Heverlee, Belgium

ARTICLE INFO

ABSTRACT

The vertical ground heat exchangers (GHE) are the most common application of the ground source heat pump (GSHP) systems. Due to ground heterogeneity and length of the boreholes, the heat exchangers cross usually several geological layers. However, in most of the current analytical models for GHEs, the restrictive assumption of ground homogeneity is considered. In this paper, a finite line-source model is proposed for GHEs that takes into account not only thermal conduction but also advection and dispersion mechanisms, induced by ground water flow, in a multilayer porous medium. Firstly, the anisotropy is added to the moving finite line-source (MFLS) model, and an existing composite model approach is modified. The temperature comparison with the numerical model results demonstrates the suitability of the approach. The proposed model provides faster solution than typical 3D numerical methods Furthermore, the homogeneous and multilayer assumptions are analyzed in dimensionless form to check the convenience of both of the approaches. The results demonstrate that, in case of high groundwater velocity in one layer, the thermal interaction with the neighboring layers decreases due to strong groundwater flow suppressing the thermal flux interaction. In that case, the prediction of homogeneous assumption is slightly sufficient in the middle of the layer. Otherwise, the multilayer approach is more appropriate in transient conditions, particularly, at the interface of layers.

1. Introduction

As an alternative and renewable energy source, the shallow geothermal energy evolves as one of the most popular energy source due to its easy accessibility and availability around the world. The ground source heat pump (GSHP) systems are the most frequent applications for extracting the energy from the shallow subsurface. As the heat extraction capacity of the GSHP system applications arises, the energy deficiency of the ground and the planning of the ground heat exchangers (GHE), which is the connected part of the system in the ground, become more important.

The market of the shallow geothermal energy (SGE) system technologies grows due to the promotion of its renewable energy source and regarding to the environmental structural policies of the governing institutions to mitigate the climate change (Bayer et al., 2012). Therefore, the long-term thermal energy efficiency of both of the system and the underground becomes of paramount importance to improve the operation performance of ground source heat pumps and to fulfill the required environmental policies.

In order to evaluate the necessary drilling depth and the regulation of the heat carrier fluid temperature, the specific heat extraction rate should be optimized regarding the characteristics of the hydro-geological conditions and the thermal properties of the ground for the long term operational effects (Bayer et al., 2014). For the planning and the design of GHE installations, the engineering guidelines (Stauffer et al., 2013; Kavanaugh and Rafferty, 2014; VDI-Richtlinie, 2001), thermal optimization methods (Hecht-Méndez et al., 2013; Sivasakthivel et al., 2014) and the software programs (de Paly et al., 2012; Blomberg et al., 2015) provide some tools to determine the length of the GHE and the optimization of the specific heat extraction rate depending on the heat demand.

For shallow geothermal system design and planning, the analytical heat source models demonstrate efficient performance compared to 3D numerical simulations that demand large computational efforts. However, the main limitation of available finite line-source and cylindrical source analytical solutions described in the literature is that

the thermal characteristics and the hydro-geological conditions of the ground are assumed uniform along the vertical depth of a GHE (Deerman and Kavanaugh, 1991; Eskilson, 1987; Zeng et al., 2002; Sutton et al., 2003; Diao et al., 2004; Marcotte et al., 2010; Man et al., 2010; Molina-Giraldo et al., 2011a; Erol et al., 2015). In reality the GHE may cross different layers along the depth with different hydro-geological and thermal properties for each layer. Therefore, the homogeneous assumption can lead unreliable results. In particular, to evaluate the long-term performance of the system, the consideration of the ground heterogeneity may allow the prediction of possible exhaustion of the heat reservoir in low conductive geological layers.

In order to evaluate the impact of multilayer ground conditions, several numerical investigations have been performed for short-term thermal response test (TRT) evaluations (e.g. a couple of days) (Signorelli et al., 2007; Lee, 2011; Florides et al., 2013; Raymond and Lamarche, 2013; Radioti et al., 2016). Lee (2011) developed a numerical (finite difference) multilayer model only for conduction, and according to their conclusion the traditional line-source models which assume homogeneous media are sufficient to estimate the ground thermal properties for the TRTs. Florides et al. (2013) presented a 3D numerical model (finite element method) which accounts only for conductive media to evaluate the fluid temperature along the length of a GHE. Signorelli et al. (2007) performed 3D numerical model to examine the influence of vertical heterogeneities along the length of a GHE during the operation of TRTs. They concluded that the heterogeneity may play an important role on the global behavior of GHE, particularly, if the groundwater flow is larger than 0.1 m per day.

Analytical method for multilayer heat transfer system requires additional complexities due to the combined boundary conditions and interactions between each layer. Several analytical models have been proposed to overpass the drawback for multilayer media (Ma and Chang, 2004; Abdelaziz et al., 2014; Sutton et al., 2002). Sutton et al. (2002) developed a multilayer algorithm by using the cylinder source model for only conduction mechanism and the algorithm requires additional data such as the downward and the upward temperatures of the heat carrier fluid, at each layer. Ma and Chang (2004) proposed an analytical solution for anisotropic multilayer media for heat conduction problems by using the linear coordinate transformation method. Abdelaziz et al. (2014) introduced a finite line-source model for vertical GHEs embedded in multilayer media. The method considers the calculation in two segments. (i) The first segment represents the layer in which the observation point is located. The finite line-source is taken into account in that layer with its depth coordinates. (ii) The second

segment considers a single point-source located in each other layer and subjected to the geometric distances between the considered observation point and the point-source from both the real and the imaginary parts of the other layers. The thermal properties of different layers are taken into account in this segment as a composite model. The method provides fruitful results, however, considers only conduction.

An analytical solution that accounts for multilayer porous media with the groundwater flow and the anisotropy is of significant interest to evaluate the temperature change in the vicinity of the GHE, which is important for the planning in long-term operations. Furthermore, the prediction of the heat exchange rate in different layers may help also to optimize the design of the system by adapting the length of GHE as a function of the thermal characteristics of the geological layers. Our objective is to extend the capability of the existing composite method of Abdelaziz et al. (2014) by taking into account the groundwater flow and the anisotropy in different layers. We solve the Green's function which is the solution of the heat conduction/advection/dispersion equation in porous media and apply the method of images for a finite length of the line-source. Afterwards, the model is subdivided into segments with the multilayer approach to deduce the temperature evolution in the different layers along time. The developed model is validated by comparison with the results obtained from the finite element software COMSOL Multiphysics. Furthermore, we investigate the importance of this multilayer effect through a dimensionless comparison between homogeneous and multilayer configurations.

2. Analytical model for multilayer ground

2.1. Finite line-source model with groundwater flow and anisotropy

The general solution of the moving finite line-source (MFLS) model is already described by Molina-Giraldo et al. (2011a). Here in this section our contribution is to take into account the thermal anisotropy that may be induced by the groundwater flow.

The governing equation of the heat conduction/advection/dispersion in porous media is given as follows (Metzger, 2002):

$$\rho_m c_m \frac{\partial T}{\partial t} = \left(\lambda_x \frac{\partial^2 T}{\partial x^2} + \lambda_y \frac{\partial^2 T}{\partial y^2} + \lambda_z \frac{\partial^2 T}{\partial z^2} \right) - u_{w,x} \rho_w c_w \frac{\partial T}{\partial x} + s \tag{1}$$

in which $u_{w,x}$ is the Darcy's velocity assumed oriented in the x-direction, s is a volumetric heat source, and $\rho_m c_m$ is the volumetric heat capacity of the medium while $\rho_w c_w$ is the volumetric heat capacity of the water.

The components of effective longitudinal and transverse thermal conductivities are defined on the directions x, y and z as follows (Hopmans et al., 2002; Constantz, 2008):

$$\lambda_x = \lambda_m + \alpha_l \rho_w c_w u_{w,x} \tag{2}$$

$$\lambda_y = \lambda_z = \lambda_m + \alpha_t \rho_w c_w u_{w,x} \tag{3}$$

where λ_m is the bulk thermal conductivity of porous medium in the absence of groundwater flow, α_l and α_t are the longitudinal and transverse thermal dispersion coefficients, respectively. The thermal dispersion is a linear function of groundwater flow and relates to the anisotropy of the velocity field (Molina-Giraldo et al., 2011b; Sauty et al., 1982). The thermal dispersion coefficients depend on different components of porous media (e.g., Darcy's velocity, particle size of the media, field scale). In the literature, some empirical relationships can be found to calculate the thermal dispersion coefficients (Neuman, 1990; Xu and Eckstein, 1995; Schulze-Makuch, 2005). The complete determination of those two parameters (α_l and α_t) is out of the scope of the present study. Consequently, mean representative values have been taken for the computations.

The solution of the partial differential equation for heat transfer in porous media (Eq. (1)) is obtained from the Green's function G of a pulse point-source Q_P at the given point coordinates (x', y', z') which releases an infinite, uniform and constant amount of energy in the radial direction of an infinite porous medium (Metzger, 2002):

$$\Delta T(x, y, z, t) = \frac{G(x, y, z, t)}{\rho_m c_m} = \frac{Q_P}{8 \rho_m c_m \sqrt{\lambda_x \lambda_y \lambda_z} \left(\frac{\pi t}{\rho_m c_m}\right)^{3/2}}$$
$$\exp\left[-\frac{(x - x')^2}{\frac{4\lambda_x t}{\rho_m c_m}} - \frac{(y - y')^2}{\frac{4\lambda_y t}{\rho_m c_m}} - \frac{(z - z')^2}{\frac{4\lambda_z t}{\rho_m c_m}} \right] \tag{4}$$

Taking into account a continuous point-source with the moving source theory, it yields:

$$\Delta T(x, y, z, t) = \frac{Q_L}{8 \rho_m c_m \sqrt{\lambda_x \lambda_y \lambda_z} \left(\frac{\pi t}{\rho_m c_m}\right)^{3/2}} \int_0^t \frac{1}{(t - t')^{3/2}}$$
$$\exp\left[-\frac{(x - v_T(t - t'))^2}{4 a_x (t - t')} - \frac{y^2}{4 a_y (t - t')} - \frac{(z - z')^2}{4 a_z (t - t')} \right] dt' \tag{5}$$

in which $a_x = \lambda_x / \rho_m c_m$, $a_y = \lambda_y / \rho_m c_m$ and $a_z = \lambda_z / \rho_m c_m$. Q_L is the heat line-source input per meter depth and v_T is thermal transport velocity that can be calculated as follows (Man et al., 2010):

$$v_T = \frac{Pe \, a_x}{H} = u_x \frac{\rho_w c_w}{\rho_m c_m} \tag{6}$$

Traditionally, Péclet number is described with the mean particle size of porous medium, here we consider Péclet number respect to the GHE length giving as follows:

$$Pe = \frac{u_x \rho_w c_w H}{\lambda_x} \tag{7}$$

In order to simplify Eq. (5), we set $\varphi_{xy} = a_x / a_y$, $\varphi_{xz} = a_x / a_z$ and $a_y = a_z$, $\lambda_y = \lambda_z$, because the anisotropy is related to the groundwater flow in the x direction. It gives:

$$\Delta T(x, y, z, t) = \frac{Q_L}{8 \rho_m c_m \lambda_y \sqrt{\lambda_x} \left(\frac{\pi t}{\rho_m c_m}\right)^{3/2}} \int_0^t \frac{1}{(t - t')^{3/2}} \exp\left[-\frac{x v_T}{2 a_x} \right.$$
$$\left. -\frac{v_T^2 (t - t')}{4 a_x} - \frac{x^2 - \varphi_{xy} y^2 - \varphi_{xz} (z - z')^2}{4 a_x (t - t')} \right] dt' \tag{8}$$

Posing the following changes of variable:

$$r = \sqrt{x^2 + \varphi_{xy} y^2 + \varphi_{xz} (z - z')^2} \tag{9}$$

$$\zeta = \frac{r}{2\sqrt{a_x (t - t')}} \tag{10}$$

$$dt' = -\frac{4 \sqrt{a_x} (t - t')^{3/2}}{r} d\zeta \tag{11}$$

Eq. (8) becomes:

$$\Delta T(x, y, z, t) = \frac{Q_L}{2 \pi^{3/2} \lambda_y r} \exp\left[\frac{x v_T}{2 a_x}\right] \int_{r/(2\sqrt{a_x t})}^{\infty} \exp\left[-\zeta^2 - \frac{v_T^2 r^2}{16 a_x^2 \zeta^2} \right] d\zeta \tag{12}$$

In order to take into account the axial effect and the groundwater flow, the solution given in Eq. (12) can be applied for the response of a constant line-source with finite length H along the vertical z direction with a pulse heat extraction after applying the method of images (Carslaw and Jaeger, 1959) by integrating Eq. (12) along the z-axis (Molina-Giraldo et al., 2011a). The moving finite line-source with the anisotropy (MFLSA) can be given as:

$$\Delta T(x, y, z, t) = \frac{q_L}{2 \pi \lambda_y} \exp\left[\frac{x v_T}{2 a_x}\right] \left[\int_0^H f(x, y, z, t) dz' \right.$$
$$\left. - \int_{-H}^0 f(x, y, z, t) dz' \right] \tag{13}$$

where:

$$f(x, y, z, t) = \frac{1}{r \sqrt{\pi}} \int_{r/(2\sqrt{a_x t})}^{\infty} \exp\left[-\zeta^2 - \frac{v_T^2 r^2}{16 a_x^2 \zeta^2} \right] d\zeta \tag{14}$$

From this point, the function $f(x, y, z, t)$ can be solved as setting a new change of variable $\Phi = \zeta^2$. The integration part of Eq. (14) is expressed as the generalized incomplete gamma function, which is given as exponential and complimentary error functions as follows:

$$f(x, y, z, t) = \frac{1}{4r} \left[\exp\left(-\frac{v_T r}{2 a_x}\right) erfc\left(\frac{r - v_T t}{2 \sqrt{a_x t}}\right) + \exp\left(\frac{v_T r}{2 a_x}\right) erfc\left(\frac{r + v_T t}{2 \sqrt{a_x t}}\right) \right] \tag{15}$$

Let's note that, as the time approaches to infinity, the steady state solution of Eq. (14) can be given as:

$$\Delta T_{ss}(x, y, z, t) = \frac{q_L}{2 \pi \lambda_y} \exp\left[\frac{x v_T}{2 a_x}\right] \left[\int_0^H \frac{1}{r} \exp\left(-\frac{v_T r}{2 a_x}\right) dz' \right.$$
$$\left. - \int_{-H}^0 \frac{1}{r} \exp\left(\frac{v_T r}{2 a_x}\right) dz' \right] \tag{16}$$

The set of Eqs. (14) and (16) can be written in dimensionless form. This has two main objectives. First, it allows to reduce the number of governing variables. Then, dimensionless form of the equations may provide us a clear understanding about the conditions which affect the heat transfer system. For instance, the Peclet number facilitates the scale-up of obtained results to the flow conditions, and the Fourier number assesses the relative importance of the heat transfer under transient conditions. The Fourier number can be given as:

$$Fo = \frac{a_x t}{H^2} \tag{17}$$

The temperature difference in dimensionless form under transient conditions can be written as:

$$\Theta(R', Z, \varphi, Fo, Pe) = 2 \exp\left[\frac{Pe}{2} R' \cos(\phi)\right] \left[\int_0^1 f(R, Fo, Pe) dZ' \right.$$
$$\left. - \int_{-1}^0 f(R, Fo, Pe) dZ' \right] \tag{18}$$

in which Fo is the Fourier number is given in Eq. (18), Pe is the Peclet

number given in Eq. (7), $R' = ((x^2 + \varphi_{xy}y^2)/H)^{1/2}$, $R = (R'^2 + \varphi_{xz}(z - Z')^2)^{1/2}$, $Z = z/H$ and $Z' = z'/H$. The parameterized form of the temperature change may help better to characterize the transport phenomena in a porous media.

The dimensionless form of the steady state solution can be given as:

$$\Theta_{ss}(R', Z, \varphi, Pe) = \exp\left[\frac{Pe}{2}R'\cos(\phi)\right]\left[\int_0^1 \frac{1}{R}\exp\left(-\frac{Pe}{2}R\right)dZ' - \int_{-H}^0 \frac{1}{R}\exp\left(-\frac{Pe}{2}R\right)dZ'\right] \qquad (19)$$

Up to here, Eq. (13) (or its dimensionless form Eq. (18)) allow to express the temperature evolution with time and (x, y, z) coordinates around GHE for a homogeneous ground including groundwater flow and thermal anisotropy. Starting from those two equations, next section describes the method to include multilayer ground.

2.2. MFLSA in multilayer ground

The principle of the multilayer finite line-source model proposed by Abdelaziz et al. (2014) for only conduction dominated heat transfer is illustrated in Fig. 1. The composite model theory is based on the geometric evaluation by taking into account the interaction of the thermal properties of one layer with the other layers. We assume that in each layer there is a heat point-source which releases an infinite and constant amount of energy, and the temperature change in a considered point is calculated in two steps. For instance, let's take the case illustrated in Fig. 1 where three layers are considered, even if this approach can be generalized for any number of layers. If the point of interest "A" is in the first layer, in the first step we take the integration limits of Eq. (13) with respect to the depth coordinates of the first layer, and the thermal properties of the first layer is directly taken. As the second step, in order to evaluate the influence of the other two layers on the observation point "A", we use again Eq. (13) by taking the integration limits with respect to the depth coordinates of the second and the third layer. The thermal properties considered in Eq. (13) are calculated as the weighted mean value of the three layers. The bulk volumetric heat capacity and

the bulk thermal conductivity are evaluated regarding to the geometric distances between the real and the imaginary heat point-sources of the second and the third layers and the observation point "A" (Appendix A). The depth coordinates of the heat point-sources in each layer is taken arbitrarily because it has no influence on the results, since we take the integration along the considered depth limits. The composite approach illustrated here for three layers can be further extended for more layers.

In order to extend this approach, it is assumed here that if the solution can be considered as a 3D affine transformation, and if the groundwater conduction/advection/dispersion phenomenon takes place in a layer, the groundwater flow can be separately taken into account in different layers. In other words, if the heat point-source can be superposed in the moving finite line-source theory, in the multilayer approach, the heat point-sources can be separately superposed in each layer as well. The interaction of the ground water flow between the layers is taken into account in terms of the heat transfer, because each layer has typically different petrophysical characteristics and the ground water advection in one layer does not affect the flow regime in adjacent layers. The model assumes distinct flow in each layer. The temperature distribution is a function of ground water advection in each layer and in the composite assumption, the effect of other layers is summed in the considered layer. Moreover, the effective thermal conductivity parameter of the composite model assumption is taken into account for the thermal interaction (Appendix A).

Consequently, the moving source theory can be updated through the following transformation matrix:

$$P(0,0,1) \times \begin{bmatrix} 1 & (x - v_T t) & 0 \\ 0 & 1 & 0 \\ 0 & 0 & -1 \end{bmatrix} \qquad (20)$$

where P is the point-source and the affine transformation includes the moving source term, as illustrated in Fig. 2.

The multilayer composite method consists essentially in the segregation of the layer for computation as a composite model and the summation of the calculated temperature differences from each layer. The first segment denotes the layer at which the point of interest is located. For instance, if the observation point is in the first layer, set as
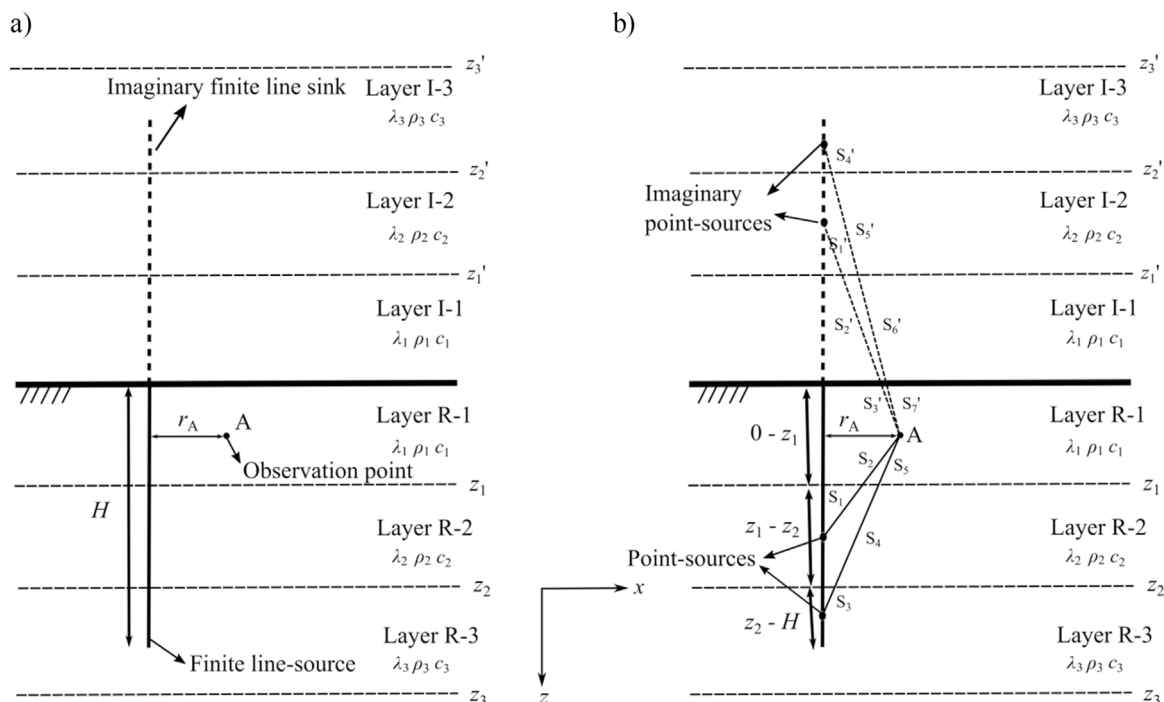

Fig. 1. The illustration of multilayer method according to Abdelaziz et al. (Abdelaziz et al., 2014) (Describing here only the observation points located in the first layer); a) GHE with a length of H passing through different layers, b) Composite model approach.

the first segment, the temperature difference is calculated based on Eq. (13) as:

$$\Delta T_1(x, y, z, t) = \frac{q_L}{2\pi\lambda_{y1}} \exp\left[\frac{xv_{T1}}{2a_{x1}}\right]\left[\int_0^{z_1} f(x, y, z, t)dz' - \int_{-z_1}^0 f(x, y, z, t)dz'\right]$$

(21)

The subscript 1 denotes the first layer and the $f(x, y, z, t)$ function is based on Eq. (16):

$$f(x, y, z, t) = \frac{1}{4r_A}\left[\exp\left(-\frac{v_{T1}r_A}{2a_{x1}}\right)erfc\left(\frac{r_A - v_{T1}t}{2\sqrt{a_{x1}t}}\right)\right.$$
$$\left.+ \exp\left(\frac{v_{T1}r_A}{2a_{x1}}\right)erfc\left(\frac{r_A + v_{T1}t}{2\sqrt{a_{x1}t}}\right)\right]$$

(22)

Note that if there is no groundwater flow in the concerned layer, the heat transport velocity v_{T1} becomes zero and the thermal diffusivity and conductivity are isotropic. Here the difference between Eqs. (13) and (21) is the integration limits which are limited to the first layer. The integration limits ([0 z_1] in this case) correspond to the depth co-ordinates of the GHE in the considered first segment layer with its imaginary part.

The effect of 2nd and 3rd layers on the 1st layer is considered in Eqs. (23) and (26), respectively. The second layer is taken into account as:

$$\Delta T_2(x, y, z, t) = \frac{q_L}{2\pi}\left[\int_{z_1}^{z_2} f_{R2}(x, y, z, t)dz' - \int_{-z_2}^{-z_1} f_{I2}(x, y, z, t)dz'\right]$$

(23)

$$f_{R2}(x, y, z, t) = \frac{1}{4\lambda_{cR2}r_A}\exp\left[\frac{xv_{T2}}{2a_{cR2}}\right]\left[\exp\left(-\frac{v_{T2}r_A}{2a_{cR2}}\right)erfc\left(\frac{r_A - v_{T2}t}{2\sqrt{a_{cR2}t}}\right)\right.$$
$$\left.+ \exp\left(\frac{v_{T2}r_A}{2a_{cR2}}\right)erfc\left(\frac{r_A + v_{T2}t}{2\sqrt{a_{cR2}t}}\right)\right]$$

(24)

$$f_{I2}(x, y, z, t) = \frac{1}{4\lambda_{cI2}r_A}\exp\left[\frac{xv_{T2}}{2a_{cI2}}\right]\left[\exp\left(-\frac{v_{T2}r_A}{2a_{cI2}}\right)erfc\left(\frac{r_A - v_{T2}t}{2\sqrt{a_{cI2}t}}\right)\right.$$
$$\left.+ \exp\left(\frac{v_{T2}r_A}{2a_{cI2}}\right)erfc\left(\frac{r_A + v_{T2}t}{2\sqrt{a_{cI2}t}}\right)\right]$$

(25)

The subscript c denotes the composite, R the real part of the geometry and I the imaginary part.

The contribution of the third layer in the second segment calculation is:

$$\Delta T_3(x, y, z, t) = \frac{q_L}{2\pi}\left[\int_{z_2}^H f_{R3}(x, y, z, t)dz' - \int_{-H}^{-z_2} f_{I3}(x, y, z, t)dz'\right]$$

(26)

$$f_{R3}(x, y, z, t) = \frac{1}{4\lambda_{cR3}r_A}\exp\left[\frac{xv_{T3}}{2a_{cR3}}\right]\left[\exp\left(-\frac{v_{T3}r_A}{2a_{cR3}}\right)erfc\left(\frac{r_A - v_{T3}t}{2\sqrt{a_{cR3}t}}\right)\right.$$
$$\left.+ \exp\left(\frac{v_{T3}r_A}{2a_{cR3}}\right)erfc\left(\frac{r_A + v_{T3}t}{2\sqrt{a_{cR3}t}}\right)\right]$$

(27)

$$f_{I3}(x, y, z, t) = \frac{1}{4\lambda_{cI3}r_A}\exp\left[\frac{xv_{T3}}{2a_{cI3}}\right]\left[\exp\left(-\frac{v_{T3}r_A}{2a_{cI3}}\right)erfc\left(\frac{r_A - v_{T3}t}{2\sqrt{a_{cI3}t}}\right)\right.$$
$$\left.+ \exp\left(\frac{v_{T3}r_A}{2a_{cI3}}\right)erfc\left(\frac{r_A + v_{T3}t}{2\sqrt{a_{cI3}t}}\right)\right]$$

(28)

In these calculations, the differences between Eqs. (21), (23) and (26) are twofold: i) The integration limits which are taken with respect to the depth coordinates of the GHE in each layer. For instance, the GHE crosses vertically over along the Layer 2, the integration limits are in between the end of the Layer 1 and the beginning of Layer 3 (i.e., z_1 to z_2) and in Layer 3 the integral limit bounds from where the Layer 2 ends (z_2) to the toe of the GHE (H). ii) In Eqs. (23) and (26), the thermal properties are taken as the weighted mean value of the three layers regarding to the distances between the arbitrary heat point-source and the observation points as developed in Appendix A.

Finally, we can determine the temperature difference at the observation point that is located in the first layer as:

$$\Delta T_A(x, y, z, t) = \underbrace{\Delta T_1}_{First segment} + \underbrace{\Delta T_2 + \Delta T_3}_{Second segment}$$

(29)

If the observation points are shifted to the second layer, then the second layer becomes the first segment, and the first and the third layers can be considered as in the second segment calculation. The observation points in the third layer can be evaluated with the similar principle. Fig. 3 shows a sketch demonstrating how the segments are separated for layers for the meaning of ΔT_1, ΔT_2 and ΔT_3.

2.3. Boundary conditions

In a real case, the heat extraction rate is not necessarily distributed uniformly along the length of a GHE, since it depends on the thermal properties of each layer. In practice, only the inlet temperature is regulated based on the demanded total amount of heat to be extracted. However, this Neumann boundary condition with constant heat flux over the vertical length of a GHE is a traditional assumption of the line/cylinder-sources model as that has been tested over decades. Eskilson (1987)) and Gehlin (2002) compared the results obtained according to that Neumann condition with experimental and numerical data of a time dependent Dirichlet boundary condition and showed that both conditions give very similar results. According to Eskilson (1987), a reasonable approximation is to use the mean value of the inlet and outlet fluid temperatures as an approximately constant fluid temperature. The reason is that the flow regime of the circulating fluid is always set to turbulent flow which drives the heat transfer system to distribute the heat exchange rate relatively constantly all along the GHE. Moreover, BniLam and Al-Khoury (2017) recently developed an advanced numerical tool to evaluate the fluid temperature along the depth of GHE (100 m vertical length) in multilayer ground conditions by fixing inlet temperature of the GHE. According to the results of BniLam and Al-Khoury (2017), the circulating fluid temperature reaches to equilibrium after a couple of hours and do not show any significant variation along the depth. This also shows that the assumption of uniform heat exchange rate can be acceptable. Although, the assumption of the
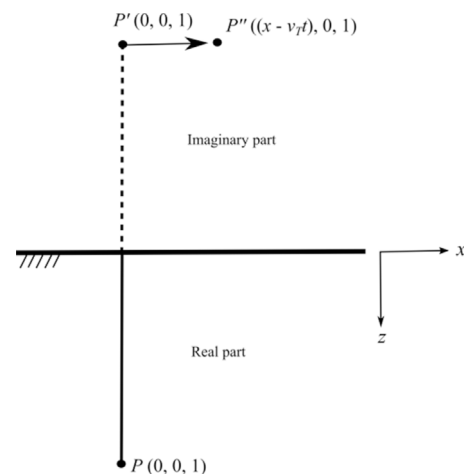

Fig. 2. The illustration of the affine transformation of a point-source. Due to the groundwater flow in x direction the imaginary part is shifted in the x direction.
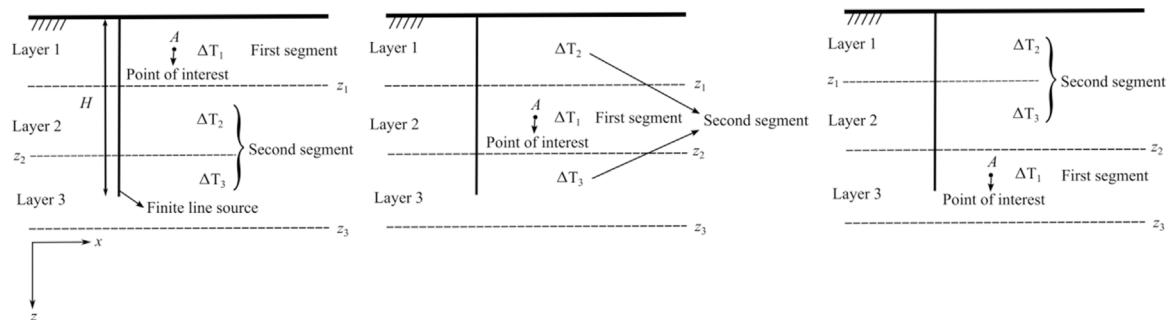
Fig. 3. Illustration of the segments for the calculation of temperature in layers.

predefined uniform heat exchange rate still may lead to overestimation for lower thermal conductivity of the ground and underestimation for higher thermal conductivity of the ground.

The ground surface temperature is assumed constant, because the integration limit of the analytical model fixes the heat flux at the co-ordinates $z = 0$ m.

3. Numerical model

The developed multilayer analytical model is validated by comparison with solution obtained from a 3D numerical model of a single line-source with a length of 50 m.

The execution time of a numerical model depends on the extension of the model domain and the size of the elements. Therefore, an appropriate time and space discretization must be determined in order to decrease computational time, as well as to avoid any influence of the boundary conditions on the numerical simulations. Three models with different dimensions have been compared under strong groundwater flow. After some numerical investigations of an appropriate temporal and spatial discretization, a model domain of $(x = 100$ m$) \times (y = 100$ m$) \times (z = 100$ m$)$ is determined for the simulations. The initial and boundary conditions are set according to the considered two different scenarios as described in the following section. In numerical model, the magnitude of the groundwater flow is set simply into the advection term of the heat equation, and the dispersion is considered in a diagonal matrix of the thermal conductivity parameter as described in Eqs. (2) and (3).

The mesh is generated using tetrahedral elements. The heat line-source is placed vertically at the central position of the model domain $(x = 50$ m, $y = 50$ m$)$. In order to get a better resolution of the temperature variations around the line-source, close to it the mesh is refined.

As the boundary conditions, we set a constant continuous heat extraction over time along the length of the GHE. The simulation time is 30 years. The initial temperature in the full domain is fixed arbitrarily to 0 °C, such as the surface temperature. Relative temperature changes in the subsurface are observed. The Backward Euler time marching method with RMS error tolerance of 10^{-3} is applied. Table 1 provides a summary of the model setup.

4. Validation results

In this section, the results obtained from the numerical models are compared with the proposed analytical solution of multilayer system (MFLSA-Multilayer) which can take into account the groundwater flow and the anisotropy in different layers.

4.1. Scenarios

The illustration setup of the scenarios can be seen in Fig. 4. We assumed two different scenarios, each of them being composed of three layers with different thermal and hydraulic characteristics. The heat

extraction rate is set uniformly to -30 W/m along the length of the line-source during 30 years.

The thermal properties of the three layers for two different scenarios are given in Table 2. The thermal dispersion is taken into account in the layers with a groundwater flow, leading to anisotropic thermal conductivity of the medium, as described in Eqs. (3) and (4). In Scenario 1, we considered a porous medium of three layers, with different magnitudes of the flow velocity. The first layer has lower groundwater flow, and the magnitude of the groundwater flow as well as the thermal properties increase from the first layer to the third layer (Table 2). In Scenario 2, we considered that the first layer is a poorly conductive soil, the second layer is with the groundwater flow, and the third layer is a highly conductive and impermeable layer.

4.2. Results

The temperature comparison over depth profile of Scenario 1 and Scenario 2 at the distances of 0.5 m and 2 m away from the borehole axis (in the direction of the flow) shown in Fig. 5 demonstrates that the numerical results agree with the proposed model after 30 years of continuous heat extraction. In addition, the fundamental solution of the analytical approach with the homogeneous assumption (i.e. MFLSA Eq. (13)) is also compared with the multilayer model. For the homogeneous assumption of MFLSA model, three cases are considered with the thermal properties of each layer taken separately. When the homogeneous solution is compared with the multilayer model, we may observe that the matching is relatively good in the middle of each layer (i.e. far from the boundary of each layer. However, close to the interface of the layers, the comparison with homogeneous models does not match because of the axial thermal transfer that generates interactions between layers. Furthermore, at the toe of the GHE (at Layer 3) for Scenario 1 (Fig. 5a and c), the axial effect is not observed even after 30 years of the operation due to the strong groundwater flow in the third layer (i.e. 3×10^{-6} m s^{-1} in Scenario 1). In Scenario 2, the axial effect can be seen in the third layer where the temperature plum tends to propagate below the borehole toe, in absence of groundwater flow in that layer.

In Scenario 2 (Fig. 5b and d), the homogeneous assumption by using only the considered layer thermal properties provides satisfactory fit only in the second layer, but in the first and the third layers the

Table 1
Summary of the model setup for verification.

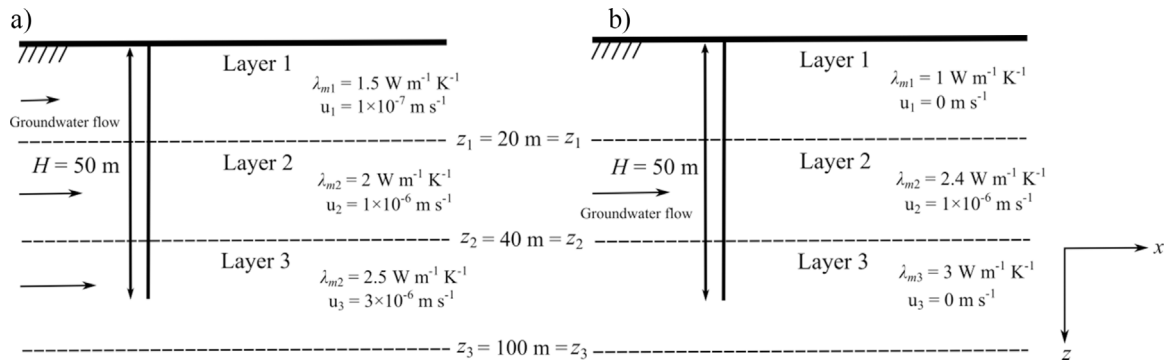| Parameter	Value
Type of problem	3D
Numerical method for heat transfer	Standard Galerkin-FEM
Simulation time	30 years
Number of elements	1,090,281
Solver type	Generalized Minimal Residual method (GMRES)

Fig. 4. Scenarios for validation of MFLSA multilayer ground model; a) Scenario 1. b) Scenario 2.

homogeneous MFLSA solution leads to overestimation. The reason is that the layer in which the groundwater advection dominates dissipates easily the temperature deficit induced by heat extraction. This effect extends to the border of the neighbor layers by thermal transfer.

The temperature result of analytical multilayer model given in Fig. 5 is slightly shifted at the interface of the layers with respect to the numerical solution. In particular, it can be seen in between Layer 1 and Layer 2. The reason can be due to the integration in the analytical model that cannot accommodate the huge temperature gradient in that zone. It can be seen that if the thermal properties and the boundary conditions of connected layers are considerably different (e.g. Layer 1 and Layer 2 in Scenario 2), the analytical solution cannot provide precise temperature gradient at the interface of the layers. On the other hand, it can be noticed that the comparison with the numerical result may not provide the real validation of the analytical model because numerical simulations is also prone to discretization approximation and computation precision. However, the good matching between the two methods may give us confidence on the validity of the developed analytical solution.

In Figs. 6 and 7, the temperature responses of the multilayer analytical model over time are compared with the numerical model results. The fundamental comparison shows that the solution of the analytical multilayer approach agrees well with the numerical results over time.

The comparison of the results between Scenario 1 and Scenario 2 (i.e. Figs. 6 and 7) shows that even the thermal properties and flow conditions are changed in Layer 1 and Layer 3, it seems that the thermal transfer system of Layer 2 under strong groundwater flow is not affected by the other layers ($u_x = 1 \times 10^{-6}$ m s^{-1}). In addition, the comparison results of Layer 1 between Scenario 1 and Scenario 2 demonstrate that the thermal transfer system of a layer in multilayer condition is also not significantly affected under low groundwater flow conditions ($u_x = 1 \times 10^{-7}$ m s^{-1}). Regarding to these results, it can be mentioned that even the thermal conductivity and flow conditions in neighboring layers are different, the thermal fluxes in a considered layer is not

considerably affected. The reason can be also accounted for the bulk volumetric heat capacities of layers which are similar between the scenarios (Table 1). To observe an impact on the thermal interaction of different layers, the storage heat capacity of a layer is also important.

Table 3 demonstrates the main advantage of the multilayer approach that provides significantly shorter calculation time compared to 3D numerical model evaluations. In particular, if the groundwater flow advection and its dispersion are considered in 3D numerical models, the computation runtime considerably increases. It can be seen that the numerical model in which the groundwater flow is considered in each layer with different magnitudes (i.e. Scenario 1) shows computation runtime more than three times larger than the Scenario 2 in which the groundwater flow is taken into account only in the second layer. Of course, the runtime of the numerical model is a function of the size of the domain and the mesh discretization. As mentioned before, we took realistic mesh size in order to obtain results which are relevant and precise enough.

5. Non-dimensional analyses

In order to analyze the convenience of the homogeneous assumption and the multilayer approach, a ratio of dimensionless temperature responses is demonstrated.

The ratio is calculated in dimensionless form of the homogeneous assumption and the multilayer approaches. As expressed in Eq. (30), the dimensionless temperature is calculated with the homogeneous MFLSA equation (Eq. (18)) with the thermal properties of the ith layer of the multilayer model of scenarios and divided by the dimensionless temperature responses of each corresponding i^{th} layer calculated with multilayer solution.

$$\Theta_{ratio} = \frac{\Theta_{MFLSA-Homogeneous-Layer_i}}{\Theta_{Multilayer-Layer_i}}$$

(30)

For instance, the dimensionless temperature is evaluated at the

Table 2
Initial input parameters for the considered scenarios.

Parameters	Scenario 1			Scenario 2		
	Layer 1	Layer 2	Layer 3	Layer 1	Layer 2	Layer 3
λ_m (W m^{-1} K^{-1})	1.5	2	2.5	1	2.4	3
u$_x$ (m s^{-1})	1×10^{-7}	1×10^{-6}	3×10^{-6}	0	1×10^{-6}	0
λ_x (W m^{-1} K^{-1})[a]	1.92	6.2	15.1	1	6.6	3
$\lambda_y = \lambda_z$ (W m^{-1} K^{-1})[a]	1.52	2.42	3.75	1	2.82	3
ρ_m (kg m^{-3})	1600	2000	2000	1500	2000	2000
c_m (J kg^{-1} K^{-1})	1200	1300	1500	800	1400	1500
(α_l)[b]	1			1		
(α_t)[b]	0.1			0.1		

[a] Calculated values according to Eqs. (2) and (3).
[b] Values taken from (Hecht-Méndez et al., 2013) to calculate effective thermal conductivities.
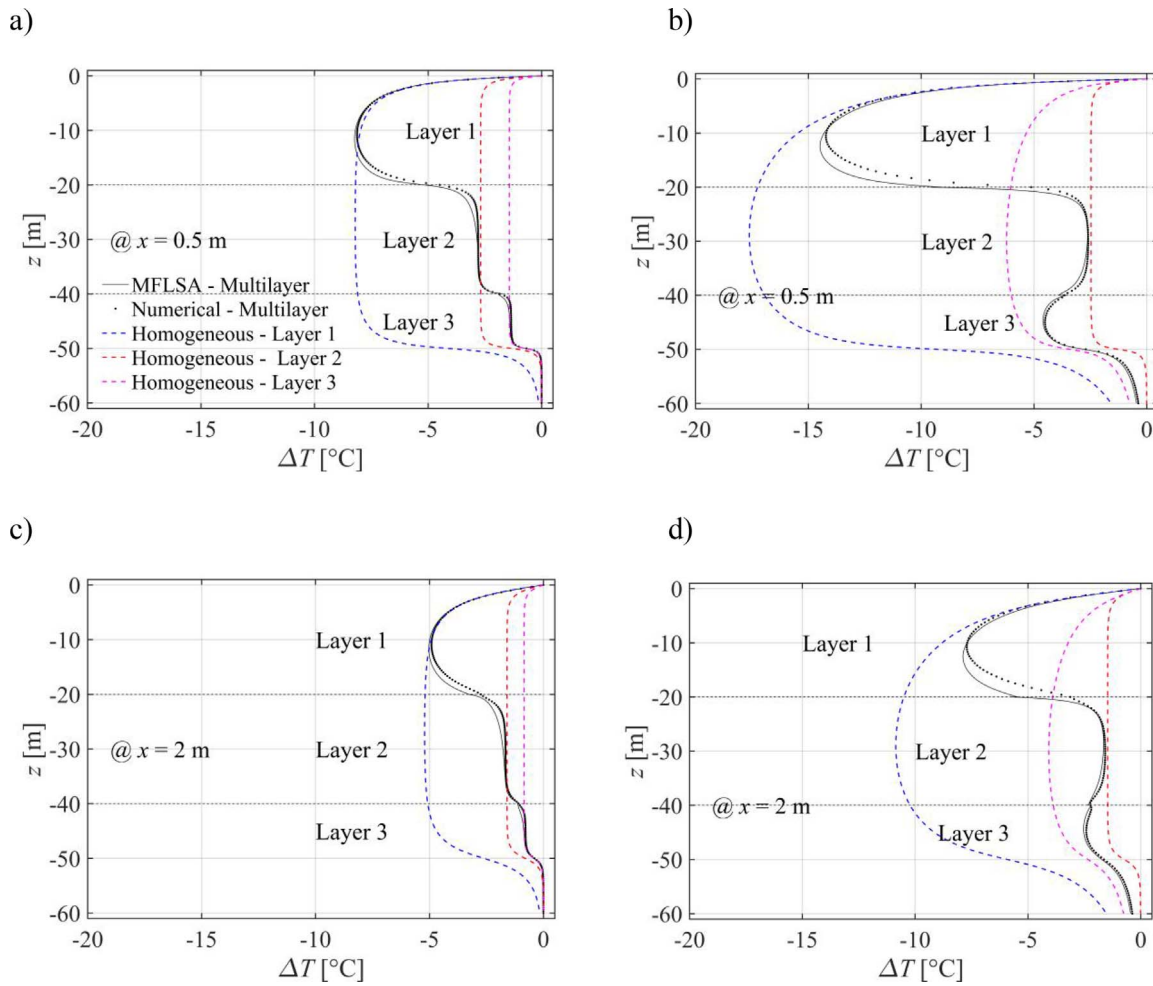
a)

b)

c)

d)

Fig. 5. Temperature results of scenarios compared with numerical and homogeneous assumption versus depth after 30 years at the coordinates (x = 0.5 m, 2 m, y = 50 m, **z**). a) and c) Scenario 1; b) and d) Scenario 2. a) and b) at a distance of 0.5 m, c) and d) at a distance of 2 m from the borehole axis in the direction of the flow. The MFLSA (Eq. (14)) is used to evaluate the temperature response of the ground with the thermal properties of each layer individually (Blue, red and magenta plots). (For interpretation of the references to colour in this figure legend, the reader is referred to the web version of this article.)

distance of $x = 0.5$ m with the homogeneous MFLSA equation (Eq. (18)) with the thermal properties of Layer 1, and divided by the dimensionless temperature of the Layer 1 of one of the scenarios calculated with multilayer approach. A perfect matching between homogeneous and multilayer cases correspond to a ratio of dimensionless temperature equals to one.

In common evaluation of the results shown in Fig. 8, the ratio of dimensionless temperature responses demonstrates that in the early time of the operation (for low Fourier number) the divergence between homogeneous and the multilayer models is larger. Over time (i.e. after 30 days), the results of these two assumptions slightly converge where the point of interests are in the middle of the layers. The reason can be
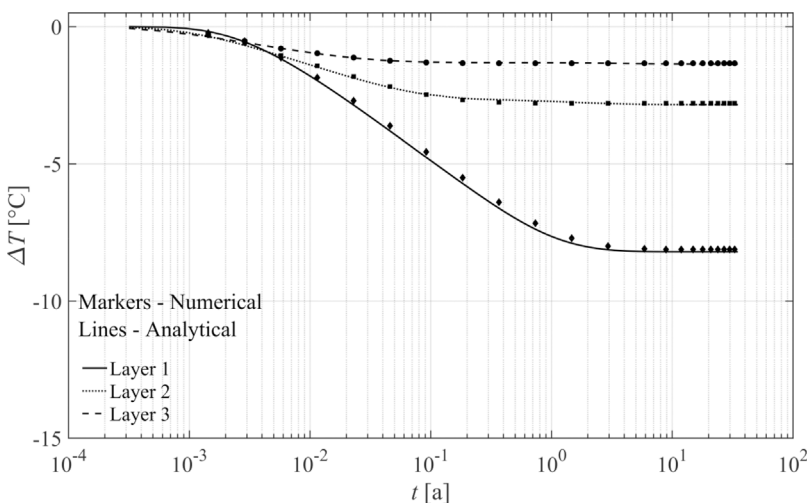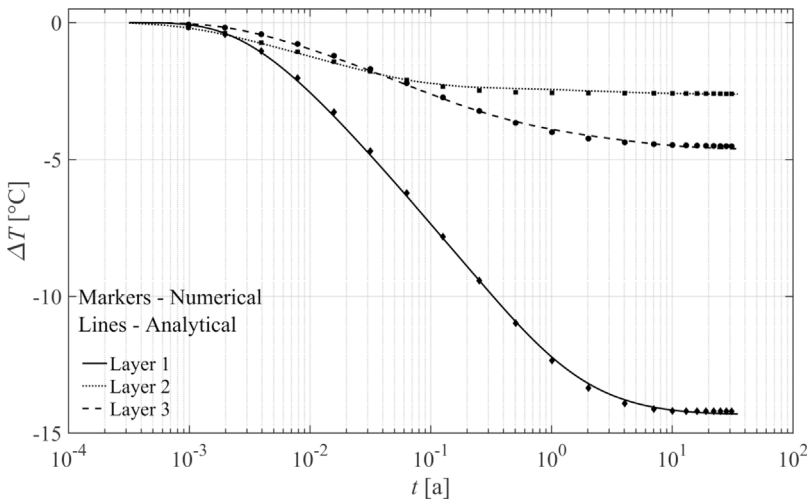
Fig. 6. Validation of analytical solution with numerical results for scenario 1 for temperature response over time at (x = 0.5 m, y = 0 m, z = 10, 30, 45 m H = 50 m).

Fig. 7. Validation of analytical solution with numerical results for scenario 2 for temperature response over time at ($x = 0.5$ m, $y = 0$ m, $z = 10, 30, 45$ m H = 50 m).

Table 3
Comparison the execution times.

Model	Runtime [s] [a]
Analytical MFLSA-Multilayer model for both of the scenarios	3 [b]
Numerical model (FEM) Scenario 1	28372
Numerical model (FEM) Scenario 2	7849

[a] Hardware specifications: Intel, 4 core i-5 3.10 GHz, RAM: 16 GB.
[b] Calculation for the coordinates ($x = 50.5$ m, $y = 50$ m, $z = 10, 30, 45$ m) (Figs. 7 and 8).

accounted for the groundwater flow which leads to reach quickly to an equilibrium of the heat transfer system of the considered layer close to the GHE. Therefore, the homogeneous assumption still provides a good prediction in the middle of a layer if separately taken into account. In contrast, the ratio results close to the interface of the layers show discrepancy all over time (Fig. 8c and d). If the point of interest is located at $x = 5$ m away from the line-source (Fig. 9), the divergence between homogeneous and multilayer approaches increases, particularly, at the interface of the layers. To predict the relative temperature change via
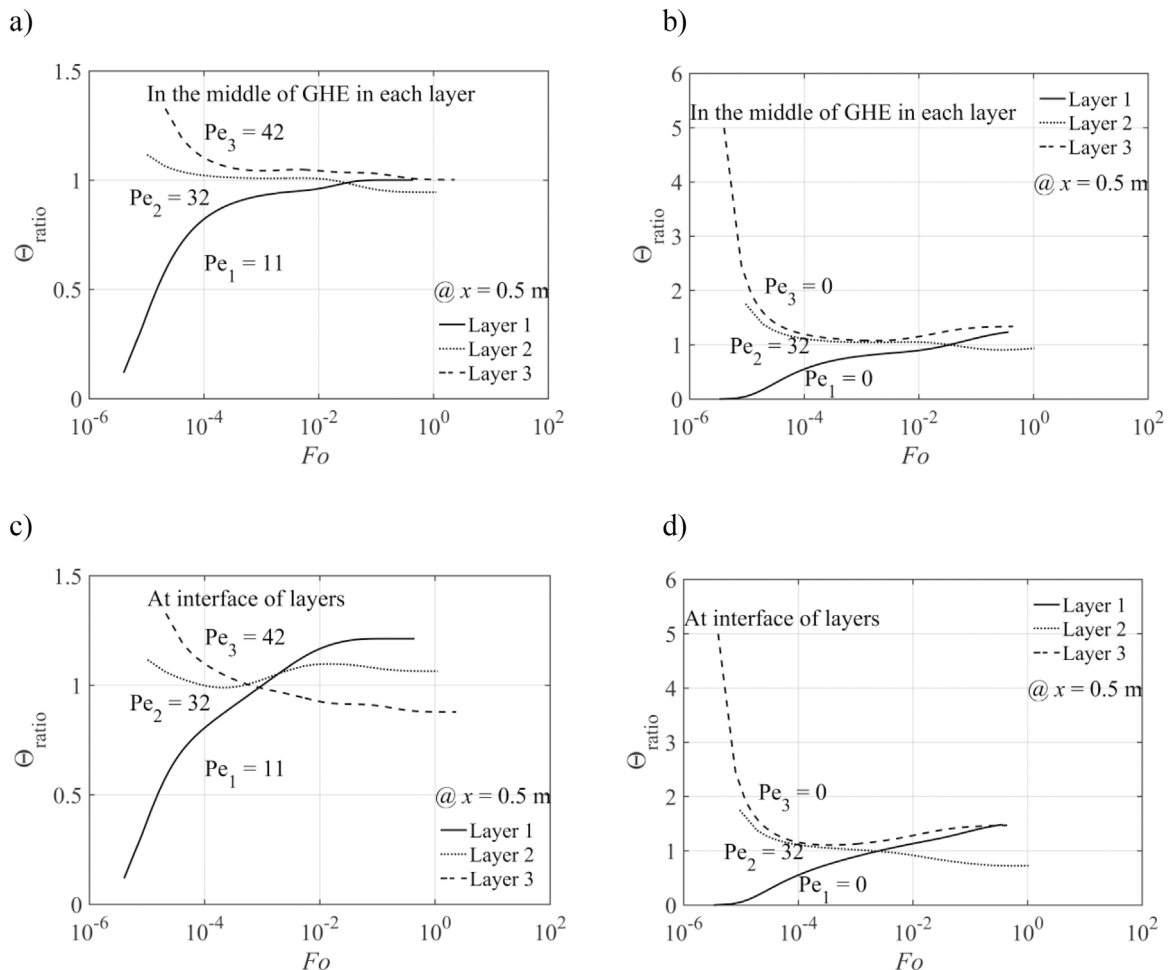

Fig. 8. The dimensionless temperature ratio of each layer between homogeneous assumption and the multilayer approach: a) and c) Scenario 1; b) and d) Scenario 2. a) and b) at ($x = 0.5$ m, $y = 0$ m, $z = 10, 30, 45$ m H = 50 m), b) and c) at ($x = 0.5$ m, $y = 0$ m, $z = 19, 39, 41$ m H = 50 m).
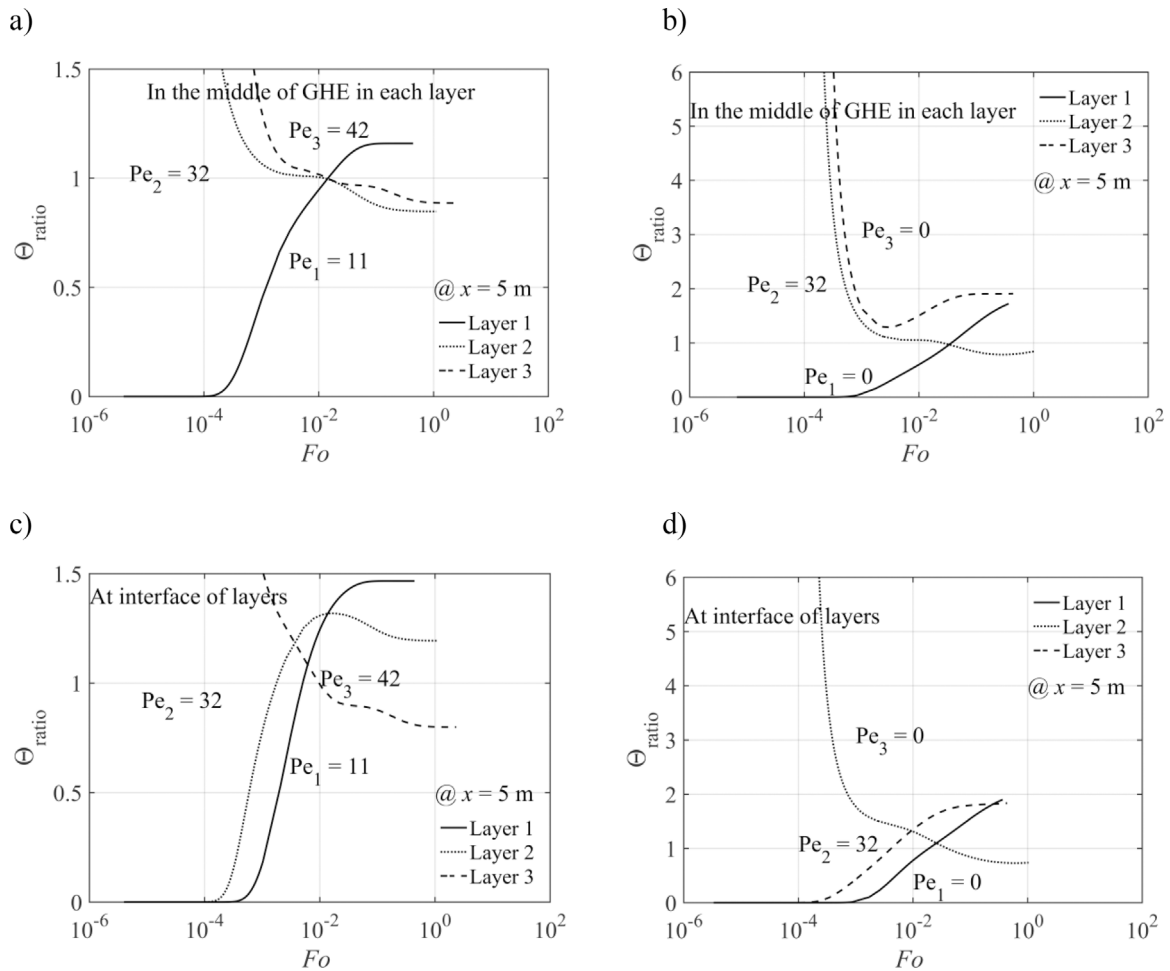
a)

b)

c)

d)

Fig. 9. The dimensionless temperature ratio of each layer between homogeneous assumption and the multilayer approach: a) and c) Scenario 1; b) and d) Scenario 2. a) and b) at (x = 5 m, y = 0 m, z = 10, 30, 45 m H = 50 m), b) and c) at (x = 5 m, y = 0 m, z = 19, 39, 41 m H = 50 m).

homogeneous MFLSA assumption by using each layer conditions separately may provide reasonable approximation only in the middle of the layers and considerably close to the GHE (e.g. $x = 0.5$ m). If the point of interest is close to the interface between layers and far from the GHE (e.g. $x > 0.5$ m), the homogeneous model will not be sufficient. This is mainly noticeable when the contrast of thermal properties between two layers is high.

6. Conclusion

The GSHP system is the most usual application of the shallow geothermal energy. It allows reducing the energy consumption for the space heating with respect to the traditional fossil fuel systems, because the ground provides the larger amount of the required energy. An analytical model that takes into account the multilayer medium with the groundwater flow and thermal anisotropy is of great interest to optimize the performance of GSHP systems.

A finite line-source analytical model is proposed that takes into account the groundwater flow and anisotropy in a multilayer medium. Firstly, we solved the Green's function of heat transfer equation that takes into account the advection and dispersion in a porous medium, and modified the composite model of a finite heat line-source suggested by Abdelaziz et al. (2014) that considered only conduction dominated medium. Furthermore, the heat exchange rate is estimated in different layers based on the composite thermal resistance model.

The finite line-source analytical solution for multilayer media provides suitable results with the addition of advection/dispersion terms, and the model provides a significant reduction of computation time in regards with conventional numerical models. As a result for Peclet numbers lower that 10 (i.e. for low ground water flow), the axial effect becomes important in layers. If the Peclet number is larger than 10 in a layer, the thermal interaction with the neighboring layers decreases due to strong groundwater flow suppressing the thermal flux interaction. The dimensionless analysis shows that if the homogeneous assumption is taken into account separately in each layer, the prediction of the temperature change is reasonable only in the middle of a layer close to the GHE at relatively short-term. Also, for long-term behavior, the interaction between layers is more and more predominant.

As an application, the consideration of a multilayer ground medium may provide a better prediction of the temperature evolution in the ground and can be used as a design tool to estimate the amount of heat that can be extracted from the ground with any excessive drop of temperature in the layer without the lowest thermal conductivity.

Appendix A. (Ground composite parameters for multilayer model)

In order to calculate the S geometric distances between the point-source and the considered observation point, the point-source is assumed in the middle of the length of the BHE in that layer (Fig. 1). It is also checked that the assumed location of the point-source in a layer has no influence on the results for the composite geometric distance calculations.

From second real layer to the observation point, the density of the real part of the second layer is:

$$\rho_{cR2} = \frac{1}{S_1 + S_2}(S_1\rho_2 + S_2\rho_1) \tag{A.1}$$

The heat capacity of the real part of the second layer is:

$$c_{cR2} = \frac{1}{S_1 + S_2}(S_1c_2 + S_2c_1) \tag{A.2}$$

The thermal conductivity of the real part of the second layer regarding to the weighted geometric mean value, which gives a better approximation compared to the arithmetic mean, is:

$$\lambda_{cR2} = \exp\left[\frac{S_1\ln(\lambda_{x2}) + S_2\ln(\lambda_{x1})}{S_1 + S_2}\right] \tag{A.3}$$

The thermal diffusivity of the real part of the second layer is:

$$a_{cR2} = \frac{\lambda_{cR2}}{\rho_{cR2}c_{cR2}} \tag{A.4}$$

From third real layer to the observation point, the thermal properties are:

$$\rho_{cR3} = \frac{1}{S_3 + S_4 + S_5}(S_3\rho_3 + S_4\rho_2 + S_5\rho_1) \tag{A.5}$$

$$c_{cR3} = \frac{1}{S_3 + S_4 + S_5}(S_3c_3 + S_4c_2 + S_5c_1) \tag{A.6}$$

$$\lambda_{cR3} = \exp\left[\frac{S_3\ln(\lambda_{x3}) + S_4\ln(\lambda_{x2}) + S_5\ln(\lambda_{x1})}{S_3 + S_4 + S_5}\right] \tag{A.7}$$

$$a_{cR3} = \frac{\lambda_{cR3}}{\rho_{cR3}c_{cR3}} \tag{A.8}$$

From second imaginary layer to the observation point, the thermal properties are:

$$\rho_{cI2} = \frac{1}{S_1' + S_2' + S_3'}(S_1'\rho_2 + S_2'\rho_1 + S_3'\rho_1) \tag{A.9}$$

$$c_{cI2} = \frac{1}{S_1' + S_2' + S_3'}(S_1'c_2 + S_2'c_1 + S_3'c_1) \tag{A.10}$$

$$\lambda_{cI2} = \exp\left[\frac{S_1'\ln(\lambda_{x2}) + S_2'\ln(\lambda_{x1}) + S_3'\ln(\lambda_{x1})}{S_1' + S_2' + S_3'}\right] \tag{A.11}$$

$$a_{cI2} = \frac{\lambda_{cI2}}{\rho_{cI2}c_{cI2}} \tag{A.12}$$

From third imaginary layer to the observation point, thermal properties are:

$$\rho_{cI3} = \frac{1}{S_4' + S_5' + S_6' + S_7'}(S_4'\rho_3 + S_5'\rho_2 + S_6'\rho_1 + S_7'\rho_1) \tag{A.13}$$

$$c_{cI3} = \frac{1}{S_4' + S_5' + S_6' + S_7'}(S_4'c_3 + S_5'c_2 + S_6'c_1 + S_7'c_1) \tag{A.14}$$

$$\lambda_{cI3} = \exp\left[\frac{S_4'\ln(\lambda_{x3}) + S_5'\ln(\lambda_{x2}) + S_6'\ln(\lambda_{x1}) + S_7'\ln(\lambda_{x1})}{S_4' + S_5' + S_6' + S_7'}\right] \tag{A.15}$$

$$a_{cI3} = \frac{\lambda_{cI3}}{\rho_{cI3}c_{cI3}} \tag{A.16}$$

References

Abdelaziz, S.L., Ozudogru, T.Y., Olgun, C.G., M II, J.R., 2014. Multilayer finite line source model for vertical heat exchangers. Geothermics 51, 406–416.

Bayer, P., Saner, D., Bolay, S., Rybach, L., Blum, P., 2012. Greenhouse gas emission savings of ground source heat pump systems in Europe: a review. Renew. Sustain. Energy Rev. 16 (no. 2), 1256–1267.

Bayer, P., de Paly, M., Beck, M., 2014. Strategic optimization of borehole heat exchanger field for seasonal geothermal heating and cooling. Appl. Energy 136, 445–453.

Blomberg, T., Claesson, J., Eskilson, P., Hellström, G., Sanner, B., 2015. EED: Earth Energy Design Simulation Tool Manual v3.2. Blocon.

BniLam, N., Al-Khoury, R., 2017. A spectral element model for nonhomogeneous heat flow in shallow geothermal systems. Int. J. Heat Mass Transf. 104, 703–717.

Carslaw, H.S., Jaeger, J.C., 1959. Conduction of Heat in Solids, second edition. Oxford University Press : Oxford University Press, New York, US –NY.

Constantz, J., 2008. Heat as a tracer to determine streambed water exchanges. Water Resour. Res. 44 (no. 4).

Deerman, D.J., Kavanaugh, P.S., 1991. Simulation of vertical U-tube ground −coupled heat pump systems using the cylindrical heat source solution. ASHRAE Trans. 97 (no. 1), 287–295.

Diao, N., Li, Q., Fang, Z., 2004. Heat transfer in ground heat exchangers with groundwater advection. Int. J. Therm. Sci. 43 (December (no. 12)), 1203–1211.

Erol, S., Hashemi, M.A., François, B., 2015. Analytical solution of discontinuous heat extraction for sustainability and recovery aspects of borehole heat exchangers. Int. J. Therm. Sci. 88 (no. 0), 47–58.

Eskilson, P., 1987. PhD Thesis: Thermal Analysis of Heat Extraction Boreholes. University of Lund.

Florides, G.A., Christodoulides, P., Pouloupatis, P., 2013. Single and double U-tube ground heat exchangers in multiple-layer substrates. Appl. Energy 102, 364–373.

Gehlin, S., 2002. PhD. Thesis: Thermal Response Test. Luleå University of Technology Luleå, Sweden.

Hecht-Méndez, J., De Paly, M., Beck, M., Bayer, P., 2013. Optimization of energy extraction for vertical closed-loop geothermal systems considering groundwater flow. Energy Convers. Manag 66, 1–10.

Hopmans, J.W., Šimunek, J., Bristow, K.L., 2002. Indirect estimation of soil thermal properties and water flux using heat pulse probe measurements: geometry and dispersion effects. Water Resour. Res. 38 (no. 1), 7–14.

Kavanaugh, S.P., Rafferty, K., 2014. Geothermal Heating and Cooling: Design of Ground-Source Heat Pump Systems. (Atlanta, US − GA).

Lee, C.K., 2011. Effects of multiple ground layers on thermal response test analysis and ground-source heat pump simulation. Appl. Energy 88 (no. 12), 4405–4410.

Ma, C.C., Chang, S.W., 2004. Analytical exact solutions of heat conduction problems for anisotropic multi-layered media. Int. J. Heat Mass Transf. 47 (April (no. 8)), 1643–1655.

Man, Y., Yang, H., Diao, N., Liu, J., Fang, Z., 2010. A new model and analytical solutions for borehole and pile ground heat exchangers. Int. J. Heat Mass Transf. 53 (June (no. 13)), 2593–2601.

Marcotte, D., Pasquier, P., Sheriff, F., Bernier, M., 2010. The importance of axial effects for borehole design of geothermal heat-pump systems. Renew. Energy 35 (April (4)), 763–770.

Metzger, T., 2002. PhD Thesis (in French): Dispersion Thermique en Milieux Poreux: Caractérisation expérimentale par Technique Inverse. Institut national polytechnique de Lorraine (INPL), Nancy.

Molina-Giraldo, N., Blum, P., Zhu, K., Bayer, P., Fang, Z., 2011a. A moving finite line source model to simulate borehole heat exchangers with groundwater advection. Int. J. Therm. Sci. 50 (December (no. 12)), 2506–2513.

Molina-Giraldo, N., Bayer, P., Blum, P., 2011b. Evaluating the influence of thermal dispersion on temperature plumes from geothermal systems using analytical solutions. Int. J. Therm. Sci. 50 (no. 7), 1223–1231.

Neuman, S.P., 1990. Universal scaling of hydraulic conductivities and dispersivities in geologic media. Water Resour. Res. 26 (no. 8), 1749–1758.

Radioti, G., Delvoie, S., Charlier, R., Dumont, G., Nguyen, F., 2016. Heterogeneous bedrock investigation for a closed-loop geothermal system: a case study. Geothermics 62, 79–92.

Raymond, J., Lamarche, L., 2013. Simulation of thermal response tests in a layered subsurface. Appl. Energy 109 (September), 293–301.

Sauty, J.P., a. Gringarten, C., Fabris, H., Thiery, D., a. Menjoz, a. Landel, P., 1982. Sensible energy storage in aquifers: 2. Field experiments and comparison with theoretical results. Water Resour. Res. 18 (April (no. 2)), 253–265.

Schulze-Makuch, D., 2005. Longitudinal dispersivity data and implications for scaling behavior. Ground Water 43 (3), 443–456.

Signorelli, S., Bassetti, S., Pahud, D., Kohl, T., 2007. Numerical evaluation of thermal response tests. Geothermics 36 (April (no. 2)), 141–166.

Sivasakthivel, T., Murugesan, K., Thomas, H.R., 2014. Optimization of operating parameters of ground source heat pump system for space heating and cooling by Taguchi method and utility concept. Appl. Energy 116, 76–85.

Stauffer, F., Bayer, P., Blum, P., Giraldo, N.M., Kinzelbach, W., 2013. Thermal Use of Shallow Groundwater. CRC Press, New York, N.Y.

Sutton, M.G., Couvillion, R.J., Ph, D., Nutter, D.W., Davis, R.K., 2002. An algorithm for approximating the performance of vertical bore heat exchangers installed in a stratified geological regime. ASHRAE Trans. 108, 177–184.

Sutton, M.G., Nutter, D.W., Couvillion, R.J., 2003. A ground resistance for vertical bore heat exchangers with groundwater flow. J. Energy Resour. Technol. 125 (no. 3), 183.

VDI-Richtlinie, 2001. Thermal Use of the Undergorund − GSHP Systems, VDI 4640 Blatt 2. Verain Deutscher Ingenieure, VDI-Verlag Düsseldorf.

Xu, M., Eckstein, Y., 1995. Use of weighted least-squares method in evaluation of the relationship between dispersivity and field scale. Ground Water 33 (6), 905–908.

Zeng, H.Y., Diao, N.R., Fang, Z.H., 2002. A finite line-source model for boreholes in geothermal heat exchangers. Heat Transf. Res. 31 (November (no. 7)), 558–567.

de Paly, M., Hecht-Méndez, J., Beck, M., Blum, P., Zell, A., Bayer, P., 2012. Optimization of energy extraction for closed shallow geothermal systems using linear programming. Geothermics 43 (July), 57–65.